

SAG Foam EOR

Buckley-Leverett Fractional Flow Theory for Non-Newtonian Foam Rheologies
C. G. Ponners

Technische Universiteit Delft

SAG Foam EOR

Buckley-Leverett Fractional Flow Theory for Non-Newtonian Foam Rheologies

by

C. G. Ponnors

to obtain the degree of Bachelor of Science
at the Delft University of Technology,
to be defended publicly on Monday July 10, 2017 at 3:30 PM.

Student number: 4642805
Project duration: April 24, 2017 – July 10, 2017
Thesis committee: Prof. dr. W. R. (William) Rossen, TU Delft, supervisor
R. (Rodrigo) Salazar, MSc. TU Delft
Dr. A.A.M. (Anne-Catherine) Dieudonné, TU Delft

An electronic version of this thesis is available at <http://repository.tudelft.nl/>.

Contents

1	Introduction & Problem Statement	1
1.1	Introduction	1
1.2	Problem Statement	1
2	Background	3
2.1	Introduction	3
2.2	Darcy Flow Equation	3
2.3	Phase Mobility	4
2.3.1	Mobility Ratio	4
2.4	Corey Relative Permeability	4
2.4.1	Foam Relative Permeability Adjustment.	5
2.5	Continuity Equation.	6
2.6	Pressure Drop	6
2.6.1	In single phase flow	6
2.6.2	In multiphase flow	7
2.7	Fractional-Flow Theory.	7
2.7.1	Fractional Flow Equation.	8
2.7.2	Dimensionless Parameters	8
2.8	FF Mass Balance.	9
2.9	Buckley-Leverett Solution	9
2.9.1	Governing PDE.	9
2.9.2	Shock formation	10
2.9.3	Newtonian Displacement Solution.	11
3	Methodology	13
3.1	Capturing Foam Non-Newtonian Rheology	13
3.1.1	Linear Flow	13
3.1.2	Radial Flow	13
3.2	Semi-Empirical Solution Method.	14
3.2.1	Space-Time Diagram Solution Algorithm	14
3.2.2	Time Rediscritization	15
3.2.3	Dimensionless Pressure Calculation	15
4	Results	17
4.1	Newtonian Case	18
4.2	Shear Thickening Case	20
4.3	Shear Thinning Case.	22
5	Discussion and Conclusions	25
	Bibliography	27

Introduction & Problem Statement

1.1. Introduction

Foam injection as a technique for mobility control has potential for beneficial application in a wide variety of enhanced oil recovery (EOR) operations. Foams can be used for diversion in acid treatments or gas injection processes [6, 14]. Foams can serve as mobility control agents in both miscible and immiscible floods and are even being tested in thermal floods [9]. As of 2008, over 120 active CO₂ projects exist in the United States with 16 additional planned projects from 2008-2010. EOR gas flooding methods are often cheaper than chemical EOR methods, and with a smaller carbon footprint than thermal methods. Nitrogen injection (miscible and immiscible), hydrocarbon gas injection, and CO₂ flooding have all been used as successful EOR methods for the recovery of medium to light oils, condensates, and volatile oils, though CO₂ has been the most widely used gas EOR method in the recent decades due to the abundance of cheap, readily available CO₂ from natural sources [10]. All of these gas EOR methods, however, suffer from the same problems: poor volumetric sweep efficiency due to gravity override, reservoir heterogeneities, and viscous instabilities. SAG foam injection can help remedy some of these issues by lowering gas mobility and providing a more favorable mobility ratio while maintaining a better injectivity than other mobility control methods such as water-alternating-gas (WAG) injection [1].

1.2. Problem Statement

With the potential of SAG foam injection in the field, more work needs to be done to understand how the non-Newtonian rheologies of foam in various permeable media affect the injection process. To that end, we develop a semi-analytical fractional flow program in MATLAB to solve for injection pressure of gas into a surfactant saturated core. The program is able to handle Newtonian, shear-thinning, and shear-thickening cases at a variety of resolutions.

2

Background

2.1. Introduction

Modeling flow through porous media, whether numerically or analytically, is a crucial step in understanding how to design a Foam Enhanced Oil Recovery process with the best possible outcome. As with all physical phenomenon, the mathematical models are based on conservation equations (mass, momentum, and energy), equation of state (EOS) models that describe fluid behavior, and some empirical and constituent relations that couple macroscopic flow to the permeable medium. In this paper, flow is assumed to be isothermal and incompressible; conservation of energy and EOS models are ignored.

In this chapter, we present a brief background on the theory of flow in permeable media, especially as it pertains to foam flow and fractional-flow theory (FFT). We describe Darcy's law, phase mobility, and Corey's relative permeability functions. Modifications to relative permeability in the presence of foam are then presented. The concept of fractional-flow is introduced in both dimensional and dimensionless forms. Finally, the solution to the first-order hyperbolic partial differential equation (PDE) through the method of characteristics is presented with an outline of the Buckley-Leverett solution for a Newtonian single-slug SAG process. Unless otherwise noted, background material comes from Lake [9].

2.2. Darcy Flow Equation

While there are several models in existence for fluid flow through porous media, the most universally utilized model is known as Darcy's law [8]. Analogous to Fourier's law of heat conduction, Fick's law of diffusion, and Ohm's law, Darcy's law is an empirical relationship that relates fluid flux (superficial velocity or "Darcy" velocity) to potential gradient of the differential form

$$\vec{u} = -\frac{\vec{k}}{\mu} \cdot \nabla \Phi = \frac{\vec{k}}{\mu} \cdot \nabla \{P - \rho g D_z\} \quad (2.1)$$

where \vec{u} is the fluid's superficial velocity vector, \vec{k} is the medium's permeability tensor, μ is the fluid viscosity, and Φ is fluid potential. Fluid potential includes a pressure component (P) and an elevation head component ($\rho g D_z$) where ρ is fluid density, g is the universal gravitational constant, and D_z is a positive distance below some horizontal reference plane. In a radial coordinate system describing 1D flow ignoring the effects of gravity, (2.1) reduces to

$$u = \frac{Q}{A_r} = -\frac{k}{\mu} \frac{\partial P}{\partial r} \quad (2.2)$$

where Q is volumetric flow rate and A_r is radial flow area. Assumptions underlying Darcy's law are laminar Stokes flow (low Reynolds number), Newtonian fluid rheology, no-slip boundary conditions within the porous media, and no chemical interactions between fluid and the porous media in question. For multiphase flow, the Darcy equation can be adapted by adding a relative permeability term k_{rj} .

$$u_j = \frac{Q_j}{A_r} = -\frac{k_{rj} k}{\mu} \frac{\partial P_j}{\partial r} \text{ for } j = 1 \dots N \text{ phases.} \quad (2.3)$$

Relative permeability is a dimensionless rock-fluid property which characterizes the inhibition of flow when multiple phases are present in a medium. It represents the ratio of effective permeability of a phase at a given saturation to the absolute permeability of the medium to some reference fluid (typically 100% air or water). It is a strong function of phase saturation, and a weak function of pore size distribution and the preference of phase j to wet the permeable medium.

2.3. Phase Mobility

Perhaps the more important parameter to an injection based EOR process, more than just relative permeability, is mobility. Mobility describes the ability for a phase to move through a permeable media when under the influence of a pressure gradient. It is the quotient between phase permeability, effective permeability, and phase viscosity. For a phase j , it is defined as

$$\lambda_j(S_j) = \frac{k_j(S_j)}{\mu_j} = \frac{kk_{rj}(S_j)}{\mu_j} = k\lambda_{rj}(S_j) \quad (2.4)$$

where λ_j is absolute phase mobility and λ_{rj} is relative phase mobility. The total relative mobility is then defined as the sum of the relative mobilities of each phase at a given water saturation as follows

$$\lambda_{rt}(S_w) = \lambda_{rw}(S_w) + \lambda_{rg}(S_w) \quad (2.5)$$

2.3.1. Mobility Ratio

Used in assessing displacement stability and sweep efficiency, mobility ratio is the quotient between the mobility of the displacing fluid and the mobility of the displaced fluid at various phase saturations. Endpoint mobility ratio (M^o) uses residual phase saturations; shock-front mobility ratio (M_{sf}) uses saturations upstream and downstream of the displacement front; and average mobility ratio (\bar{M}) uses the average water saturation behind the displacement front (\bar{S}_w) as follows

$$M^o = \frac{\lambda_{rg}^o}{\lambda_{rw}^o}; \quad M_{sf} = \frac{\lambda_{rt}^+}{\lambda_{rt}^-}; \quad \bar{M} = \frac{\lambda_{rt}^{\bar{S}_w}}{\lambda_{rt}^-}; \quad (2.6)$$

where superscripts $+$ and $-$ refer to upstream and downstream of the displacement front respectively. When mobility ratio is unity or less, the displacement is considered to be *stable*. At higher mobility ratios, the displacing phase is more mobile than the displaced phase, and former tends to finger through the latter due to viscous instabilities. Decreasing mobility ratio improves displacement efficiency, vertical sweep efficiency, and areal sweep efficiency.

2.4. Corey Relative Permeability

Almost every EOR process is highly dependent on the relative permeability of the phases in-situ. Most tertiary recovery processes fundamentally operate by modifying some property that shifts the relative permeability curves in a manner beneficial to sweep and oil recovery. While no theoretical expression exists for the relative permeability functions, Corey's semi-empirical relations are commonly used and provide smooth differentiable functions that can be fit to lab data. For two-phase flow of water and gas, the Corey's relative permeability functions are

$$k_{rw}(S_w) = k_{rw}^o \left(\frac{S_w - S_{wr}}{1 - S_{wr} - S_{gr}} \right)^{n_w} \quad S_{wr} \leq S_w \leq 1 - S_{gr} \quad (2.7)$$

$$k_{rg}(S_w) = k_{rg}^o \left(\frac{1 - S_w - S_{wr}}{1 - S_{wr} - S_{gr}} \right)^{n_g} \quad S_{gr} \leq S_g \leq 1 - S_{wr} \quad (2.8)$$

where S_w , S_{wr} , and S_{gr} refer to water saturation, residual water saturation, and residual gas saturation respectively. The terms k_{rw}^o and k_{rg}^o are endpoint relative permeabilities, i.e., the relative permeability of a phase at the irreducible saturation of the other phase. These endpoint values are dependent on

the wettability of the rock with the fluids in question.

In a typical sandstone with the gas-water system used in this paper, water is the wetting phase with gas acting as a strongly non-wetting phase. (While most rocks are water-wet and can become mixed-wet or oil-wet under the right conditions, gaseous immiscible phases are always the most non-wetting in a two or three phase system). At irreducible gas saturation, gas is trapped in isolated globules several pore diameters in length, often centering in the center of the largest pores. Wetting fluids (e.g. water), occupy crevices between rock grains and form continuous coating of the rock surfaces. From a transport perspective, the trapped non-wetting phase is a larger hindrance to the wetting phase than a trapped wetting phase is to the non-wetting phase. Thus, wetting phase endpoint relative permeability is less than that of the non-wetting phase.

With the endpoints of the curves set by S_{rj} and k_{rj} , the Corey saturation exponents n_j determine non-linearity. An exponent of one prescribes a linear relationship with higher exponents increasing the upward concavity of the curves. For the same reason as for the inequality of endpoint relative permeabilities, saturation exponents for the wetting phase tend to be larger (k_{rw} more non-linear) than for the non-wetting phase.

2.4.1. Foam Relative Permeability Adjustment

As previously mentioned, the purpose of foam injection is to use surfactant to decrease gas mobility so that a favorable mobility ratio and more efficient sweep efficiency is achieved. In previous literature, this mobility reduction is represented by a reduction in the gas relative permeability rather than an increase in gas viscosity. A common foam mobility model is that used by the Computer Modeling Group in their STARS software [7]. This model captures the reduction in gas relative permeability in the presence of surfactant through a foam mobility-reduction factor (FM). FM is a dimensionless parameter which represents the factor by which gas relative permeability is reduced due to the presence of foam relative to the gas relative permeability at the same water saturation in the absence of foam. Foam relative permeability is defined by

$$k_{rg}^f(S_w) = FM \times k_{rg}(S_w) \quad (2.9)$$

where the factor FM is defined as

$$FM = \frac{1}{1 + fmmobF_1F_2F_3F_4F_5F_6} \quad 0 \leq F_i \leq 1 \quad (2.10)$$

The parameter $fmmob$ is a reference mobility reduction factor, i.e., the maximum reduction in gas mobility a foam of a formulation can achieve. $fmmob$ is scaled by six dimensionless coefficients F_i which represent the effect of surfactant concentration, water saturation, oil saturation, capillary number, gas velocity, and critical capillary number, respectively on foam behavior.

In this paper, we focus on the F_2 function which captures the effect of water saturation on foam mobility, an important factor to foam behavior in the high quality (low S_w) regime. In SAG injection, a significant volume of the reservoir (specifically the near-wellbore region) operates in this high-quality regime, so this assumption is appropriate. FM becomes a function only of S_w in the form

$$FM(S_w) = \frac{1}{1 + fmmobF_2(S_w)} \quad (2.11)$$

STARS Model Dryout Function: In the STARS model, F_2 is defined as

$$F_2(S_w) = 0.5 + \frac{\arctan(epdry(S_w - fmdry))}{\pi} \quad (2.12)$$

$fmdry$ is the foam parameter which is the water saturation at which foam collapses and mobility reduction drastically decreases. $epdry$ controls the abruptness of foam collapse at $fmdry$. Large values give a sharp almost discontinuous transition between the two regimes, while smaller values result in a more gradual transition.

N.Z. et al. Dryout Function: The STARS model in equation (2.12) does not model full foam collapse and dryout. The foam retains some mobility reduction at all water saturations including S_{wc} . The exact behavior of high-quality foams at very low water saturations is still unclear, but recent

studies provide some evidence of a weaker foam at low water saturations than that presented in the STARS model. A model proposed by Namdar Zanganeh [11] modifies the STARS F_2 model by adding an additional term that captures the complete collapse of foam at residual water saturation.

$$F_2(S_w) = \left(0.5 + \frac{\arctan(epdry(S_w - fmdry))}{\pi} \right) - \left(0.5 + \frac{\arctan(epdry(S_{wr} - fmdry))}{\pi} \right) \quad (2.13)$$

Due to the importance of the behavior of foam in this high quality regime to well injectivity and pressure drop considerations, the N.Z. et al model for F_2 as in equation (2.13) is used throughout the rest of this paper.

In the presence of foam, all the parameters represented in equations (2.3-2.6)—Darcy velocity, mobility, relative mobility, total relative mobility, and mobility ratio—can be calculated in the same manner by replacing k_{rg} with k_{rg}^f where the superscript f indicates the presence of foam.

2.5. Continuity Equation

Conservation of mass applied to a representative elementary volume states that the net transport of mass into the volume plus external source must equal the change in total mass in the volume over an increment in time. That is,

$$\text{Mass in} - \text{Mass out} + \text{Source} = \text{Accumulation} \quad (2.14)$$

In the context of radial flow, the terms in (2.14) are

$$\text{Flow in} = 2\pi h(\rho ur)_r \Delta t \quad (2.15)$$

$$\text{Flow out} = 2\pi h(\rho ur)_{r+\Delta r} \Delta t \quad (2.16)$$

$$\text{Accumulation} = 2\pi r \Delta r h(\rho \phi)_{t+\Delta t} - 2\pi r \Delta r h(\rho \phi)_t \quad (2.17)$$

where the terms ρ , ϕ , and t are density, porosity, and time respectively. Substituting these terms into (2.14) and dividing both sides by $2\pi r h \Delta t \Delta r$ results in

$$\frac{1}{r} \frac{(\rho ur)_r - (\rho ur)_{r+\Delta r}}{\Delta r} = \frac{(\rho \phi)_{t+\Delta t} - (\rho \phi)_t}{\Delta t} \quad (2.18)$$

Taking the limit as Δr and Δt approach zero leads to the differential of the form

$$-\frac{1}{r} \frac{\partial(\rho ur)}{\partial r} = \frac{\partial(\rho \phi)}{\partial t} \quad (2.19)$$

which is the radial continuity equation. Expressed generally in 3D, the continuity expression is

$$-\nabla \cdot (\rho \vec{u}) = \frac{\partial}{\partial t}(\rho \phi) \quad (2.20)$$

The same continuity equation (2.19) can be expressed for a given phase in multiphase flow, if superficial velocity u in terms (2.15) and (2.16) is taken to be that of a single phase j and the phase saturation S_j is added into the accumulation term. Assuming incompressible fluid and matrix, dividing both sides by $2\pi \rho_j r h \Delta t \Delta r$, and taking the limit, you obtain

$$-\frac{1}{r} \frac{\partial(u_j r)}{\partial r} = \phi \frac{\partial(S_j)}{\partial t} \quad (2.21)$$

2.6. Pressure Drop

2.6.1. In single phase flow

In the case of incompressible, steady state, 1D radial flow, the continuity equation (2.20) simplifies to the form

$$\frac{\partial}{\partial r}(ru_r) = 0 \quad (2.22)$$

It follows then that ru_r is a constant dependent on some boundary condition. This implies that superficial velocity u scales inversely with radius away from the wellbore. This is also consistent with the definition of superficial velocity, i.e., a volumetric flow rate divided by flow area, where in radial coordinates, flow area is a function of radius r .

Using the definition that flow area $A(r) = 2\pi rh$, equation (2.2) can be integrated to yield the pressure difference between the wellbore radius r_w and the outer radius r_e as follows

$$\int_{P_{r_e}}^{P_{r_w}} dP = - \int_{r_e}^{r_w} \frac{Q\mu}{kA} dr = \frac{Q}{2\pi hk} \int_{r_w}^{r_e} \frac{1}{\lambda_r r} dr \quad (2.23)$$

For single phase flow, mobility is constant and integration of the RHS yields

$$P_{r_w} - P_{r_e} = \frac{Q}{2\pi hk\lambda_r} \ln\left(\frac{r_e}{r_w}\right) \quad (2.24)$$

2.6.2. In multiphase flow

In multiphase flow, the influence of a modified mobility has to be taken into account. Under the assumption of incompressible phases, the total flow rate is

$$u_t = \frac{Q_t}{A} = u_w + u_g \quad (2.25)$$

Using equation (2.3) leads to the form

$$u_t = - \left(\frac{kk_{rw}}{\mu_w} \frac{\partial P_w}{\partial r} + \frac{kk_{rg}}{\mu_g} \frac{\partial P_g}{\partial r} \right) \quad (2.26)$$

If capillarity is neglected, the pressure gradients in each phase are equivalent. Recognizing the definition of total relative mobility from equation (2.5) leads to

$$u_t = -k\lambda_{rt}(S_w) \frac{dP}{dr} \quad (2.27)$$

Integrating equation (2.27) between the wellbore radius r_w and the outer radius r_e yields

$$P_{r_w} - P_{r_e} = \frac{Q_t}{2\pi hk} \int_{r_w}^{r_e} \frac{1}{r\lambda_{rt}(S_w(r))} dr \quad (2.28)$$

2.7. Fractional-Flow Theory

Originally derived by Buckley and Leverett in 1942 for use in estimating efficiency of water floods, fractional flow theory (FFT) has proved applicable to numerous EOR processes [1, 12]. In the context of foam EOR, the process has been outlined previously in Rossen et al. [13, 15], Zhou and Rossen [16]. Fractional-flow theory provides a simple framework to make predictions about multiphase flow, capturing many dynamic displacement effects in a straight-forward analytical closed form. Several simplifying assumptions underlie the theory:

1. Flow is one-dimensional and isothermal.
2. At most there are two phases interacting simultaneously. There are no phase changes.
3. The permeable medium and all fluids are incompressible.
4. There is no chemical interaction between fluids and rock, except for chemical adsorption.
5. Steady-state mobilities for each phase are achieved instantaneously.
6. Phase viscosities are Newtonian
7. Dispersion and viscous fingering is neglected
8. Initial conditions are homogeneous throughout the medium.

2.7.1. Fractional Flow Equation

In the context two-phase flow of water and gas, fractional-flow of water f_w is defined as the fraction of water flow relative to the total fluid flow rate as follows

$$f_w \equiv \frac{Q_w}{Q_w + Q_g} = \frac{u_w}{u_w + u_g} \quad (2.29)$$

Taking equation (2.3) for water and gas phases and including the gravity term yields the system

$$-\frac{u_w \mu_w}{k k_{rw}} = \frac{dP_w}{dx} + \rho_w g \sin \alpha \quad (2.30)$$

$$-\frac{u_g \mu_g}{k k_{rg}} = \frac{dP_g}{dx} + \rho_g g \sin \alpha \quad (2.31)$$

Subtracting (2.31) from (2.30), substituting in $u_w = u f_w$ from (2.29), and rearranging yields

$$f_w = \frac{1 + \frac{k k_{rg}}{u \mu_g} \left[\frac{dP_c}{dx} - \Delta \rho g \sin \alpha \right]}{1 + \frac{k_{rg} \mu_w}{k_{rw} \mu_g}} \quad (2.32)$$

where capillary pressure $P_c = P_g - P_w$, the density difference between the two phases $\Delta \rho = \rho_w - \rho_g$, and α is the positive angle from the horizontal. If capillary pressure is negligible ($\frac{dP_c}{dx} \approx 0$) and flow is horizontal ($\alpha = 0$), then equation (2.32) can reduce to

$$f_w(S_w) = \frac{1}{1 + \frac{k_{rg}(S_w) \mu_w}{k_{rw}(S_w) \mu_g}} = \left(1 + \frac{\lambda_{rg}(S_w)}{\lambda_{rw}(S_w)} \right)^{-1} \quad (2.33)$$

In this form, the fractional flow curve depends parametrically on M^o , n_w and n_g . The S-shaped curve has an inflection point that varies with M^o . Curvature is least when M^o is unity, shifts to the left (larger f_w at given S_w) with increasing M^o , and shifts to the right (smaller f_w at given S_w) with decreasing M^o . In this way, the fractional flow curve is highly sensitive to phase viscosities and endpoint relative permeabilities.

For the foam fractional-flow curve, the gas relative mobility is replaced by the foam relative mobility as in

$$f_w(S_w) = \left(1 + \frac{\lambda_{rg}^f(S_w)}{\lambda_{rw}(S_w)} \right)^{-1} \quad (2.34)$$

2.7.2. Dimensionless Parameters

Dimensionless position: is defined as the fraction of the pore volume at a given radius back to the injection point, i.e., wellbore radius.

$$x_D(r) \equiv \frac{r^2 - r_w^2}{r_e^2 - r_w^2} \quad x_D \in [0, 1] \quad (2.35)$$

Dimensionless time: is defined as the cumulative volume injected at a given time divided by the pore volume of the reservoir. If the injection rate is constant, then dimensionless time scales linearly with physical time. Dimensionless time is sometimes referred to as *Pore Volumes (PV) Injected*.

$$t_D \equiv \int \frac{Q(t) dt}{\pi(r_e^2 - r_w^2) h \phi} \quad t_D > 0 \quad (2.36)$$

Dimensionless pressure: In order to remove the influence of reservoir permeability and simplify calculations, the dimensional pressure drop in each layer is normalized by the pressure drop of injecting water at the same volumetric rate into a fully water-saturated layer, i.e., $S_w = 1$. The resulting dimensionless pressure can be written as

$$P_D = \frac{P_{r_w} - P_{r_e}}{(P_{r_w} - P_{r_e})_{S_w=1}} = \frac{\frac{Q_g}{2\pi k h} \int_{r_w}^{r_e} \frac{1}{r \lambda_{rt}(S_w)} dr}{\frac{Q_w}{2\pi k h \lambda_{rw}} \ln\left(\frac{r_e}{r_w}\right)} \quad (2.37)$$

Assuming a water viscosity of 1 cP (10^{-3} Pa s), the relative mobility of water in a water-saturated reservoir is $1/\mu_w = 1,000 [\text{Pa} \cdot \text{s}]^{-1}$. Simplifying equation (2.37) thusly yields

$$P_D = \frac{\int_{r_w}^{r_e} \frac{1}{r \lambda_{rt}(S_w)} dr}{1000 \times \ln\left(\frac{r_e}{r_w}\right)} \quad (2.38)$$

2.8. FF Mass Balance

The continuity equation (2.21) derived previously can be written in terms of water fractional flow f_w and dimensionless parameters to form the fundamental conservation law used in Buckley-Leverett analysis. Plugging in equation (2.29) into equation (2.21) leads to

$$-\frac{1}{r} \frac{\partial(uf_w r)}{\partial r} = \phi \frac{\partial(S_j)}{\partial t} \quad (2.39)$$

As (ur) is a conserved quantity and constant with respect to radius (See subsection 2.5 on page 6), it can be taken out of the differential. Plugging in the definition of superficial velocity and rearranging yields

$$\phi \frac{\partial S_w}{\partial t} + \frac{Q_t}{2\pi r h} \frac{\partial f_w}{\partial r} = 0 \quad (2.40)$$

The derivative of dimensionless position with respect to radius is

$$\frac{dx_D}{dr} = \frac{2r}{r_e^2 - r_w^2} \quad (2.41)$$

The derivative of dimensionless time with respect to physical time is

$$\frac{dt_D}{dt} = \frac{Q_t}{\pi h \phi (r_e^2 - r_w^2)} \quad (2.42)$$

Expanding the partial derivatives in (2.40) by chain rule and plugging in equations (2.41-2.42) yields

$$\frac{Q_t \phi}{\pi h \phi (r_e^2 - r_w^2)} \frac{\partial S_w}{\partial t_D} + \frac{Q_t}{2\pi r h} \frac{2r}{(r_e^2 - r_w^2)} \frac{\partial f_w}{\partial x_D} = 0 \quad (2.43)$$

Canceling like terms leads to the mass balance equation in the dimensionless form

$$\frac{\partial S_w}{\partial t_D} + \frac{\partial f_w}{\partial x_D} = 0 \quad (2.44)$$

As can be seen in equation (2.33), water fractional-flow is a function of position and time only through its dependence on water saturation. Thus, using the chain rule to expand the f_w partial derivative in terms of a total derivative with water saturation, equation (2.44) becomes

$$\frac{\partial S_w}{\partial t_D} + \frac{df_w}{dS_w} \frac{\partial S_w}{\partial x_D} = 0 \quad (2.45)$$

2.9. Buckley-Leverett Solution

As can be seen in equation (2.33), water fractional-flow is a function of position and time only through its dependence on water saturation. Thus, using the chain rule to expand the f_w partial derivative in terms of a total derivative with water saturation, we can obtain the dimensionless governing PDE.

2.9.1. Governing PDE

The problem, therefore, is to find solutions $S_w(x_D, t_D)$ subject to the governing equation and the initial and boundary conditions

$$\frac{\partial S_w}{\partial t_D} + \frac{df_w}{dS_w} \frac{\partial S_w}{\partial x_D} = 0 \quad (2.46)$$

$$S_w(x_D, 0) = S_{wI}, \quad x_D \geq 0 \quad (2.47)$$

$$S_w(0, t_D) = S_{wJ}, \quad t_D \geq 0 \quad (2.48)$$

where I and J represent initial and injection conditions respectively.

Equation (2.46) represents a prototypical first-order hyperbolic PDE with variable coefficients. It is a one-way *wave equation* in which saturations travel with a finite speed of propagation from *source* to *sink*. Generally, it is called an *initial value problem* as no information downstream of the wave is needed for a solution. Saturation depends only on dimensionless position and time $S_w(x_D, t_D)$. Therefore, equation (2.46) can be solved through a technique known as the method of characteristics (MOC). Along a characteristic (a line in the (t, x) of—in our case—constant water saturation), the PDE is reduced to a family of ordinary differential equations (ODE) along which the solution can be integrated from some initial condition. At a constant saturation, the total derivative dS_w can be written as

$$dS_w(x_D, t_D) = \left(\frac{\partial S_w}{\partial t_D} \right)_{x_D} dt_D + \left(\frac{\partial S_w}{\partial x_D} \right)_{t_D} dx_D = 0 \quad (2.49)$$

Rearranging equation (2.49) can then yield

$$\left(\frac{dx_D}{dt_D} \right)_{dS_w=0} = - \frac{\left(\frac{\partial S_w}{\partial t_D} \right)_{x_D}}{\left(\frac{\partial S_w}{\partial x_D} \right)_{t_D}} \equiv v_{S_w} \quad (2.50)$$

where v_{S_w} is a *specific* velocity of the saturation S_w but normalized by the bulk fluid interstitial velocity u/ϕ . It is dimensionless. Eliminating either of the derivatives in equation (2.50) with (2.46) yields

$$v_{S_w} = \frac{df_w}{dS_w} = f'_w \quad (2.51)$$

which states that the specific velocity of a given saturation is equal to the derivative of the fractional flow curve at that saturation. This is the essence of Buckley-Leverett analysis. Because all saturations between S_{wI} and S_{wJ} exist at the origin of $x_D - t_D$ and a given saturation has a constant velocity, the position of any saturation at a given t_D is *te to Time*

2.9.2. Shock formation

As mentioned in subsection 2.7.1, most fractional flow curves have an inflection point dependent on endpoint mobility ratio. Equation (2.51) shows that if this inflection point is between S_{wI} and S_{wJ} , saturation specific velocity will go through a maximum between this range. The resulting solution for saturation profile can yield three values of S_w at a given x_D and t_D . While non-physical, these multiple solutions are technically mathematically valid. This type of non-physical solution is a common feature of hyperbolic equations, especially dissipation-free conservation equations which idealize natural conservation laws by neglecting dissipation, i.e., dispersion, diffusion, capillary pressure, compressibility, and thermal conductivity. While dissipative mechanisms are always present in nature, idealizing the process with a *shock* simplifies the analysis while approximating the true behavior of the phenomenon to a good extent. In our context, the *shock* is a discontinuity in saturation at the *shock front* of the displacement.

To determine the location, velocity, and magnitude of the shock front, we create a water mass balance over a control volume that contains the shock in time interval Δt

$$(\text{Water volume in}) - (\text{Water volume out}) = (\text{Water volume present finally}) - (\text{Water volume present initially}) \quad (2.52)$$

$$[f_w(S_w^+) - f_w(S_w^-)] \int_t^{t+\Delta t} q dt = [(v(t+\Delta t) - x_1)S_w^+ + (x_2 - v(t+\Delta t))S_w^-]A\phi - [(vt - x_1)S_w^+ + (x_2 - vt)S_w^-]A\phi \quad (2.53)$$

where S_w^+ and S_w^- are the water saturations upstream and downstream of the shock respectively, and x_1 and x_2 are the upstream and downstream positions of the control volume in question. Solving for specific shock velocity leads to

$$v_{sf} = \frac{f_w(S_w^+) - f_w(S_w^-)}{S_w^+ - S_w^-} \quad (2.54)$$

To be physically possible and continuous, the shock saturation must obey equations (2.51) and (2.54). The velocity of the shock front derived from mass balance must equal the velocity derived from the fractional flow curve. Setting equations (2.51) and (2.54) equal and taking the downstream water saturation to be the initial water saturation yields

$$f_w' \big|_{S_w^{sf}} = \frac{f_w(S_w^{sf}) - f_w(S_w^I)}{S_w^{sf} - S_w^I} \quad (2.55)$$

Interpreted graphically in $f_w - S_w$ space, equation (2.55) can be seen as a straight line through point (S_w^I, f_w^I) tangent to the fractional flow curve at (S_w^{sf}, f_w^{sf}) . The slope of this line is the specific shock velocity.

2.9.3. Newtonian Displacement Solution

With this background information, we can now calculate the saturation profile solution for the radial displacement of a surfactant solution by gas. Initial condition I is taken to be a porous medium fully saturated with a uniform surfactant concentration, i.e., $S_w^I = 1$ and $f_w^I = 1$. The gas injection condition J is taken to be at $S_w^J = S_{wr}$ and $f_w^J = 0$. With a fractional flow curve constructed using equation (2.33) using kr_g^f instead of kr_g , the shock point can be found by plotting a line through initial point I tangent to the fractional flow curve. The ultimate displacement follows a path along the fractional-flow curve from J smoothly to the shock point (S_w^{sf}, f_w^{sf}) ; it then jumps to the initial condition point I . At each saturation along the path, the saturation velocity is given by equation (2.51), and the shock front velocity is given by equation (2.54). At a given dimensionless time t_D , the saturation profile can be plotted with the use of equation (??) and by recognizing the fact that downstream of the front, S_w is at initial conditions.

3

Methodology

3.1. Capturing Foam Non-Newtonian Rheology

For a Newtonian foam, the FFT construction presented in section 2.9.3 is appropriate. There only two phases (gas and water with a constant surfactant concentration), relative permeability parameters are constant, and phase viscosities are constant; water fractional flow is only dependent on water saturation which is fully captured in a single fractional-flow curve. For foam with a non-Newtonian rheology, which is most commonly the case, the fractional flow construction is different and must be modified in a way to capture the effects of varying shear rates.

3.1.1. Linear Flow

In linear flow, this process is relatively simple; since flow area does not change with position, superficial velocity u also does not change and shear rate is constant throughout the core. Thus, foam mobility can be calibrated with laboratory data and calculated *a priori*. There is only one fractional-flow curve for a given injection rate. In the STARS model [7], a shear-thinning rheology is represented as a function of pressure gradient

$$F_5 = \left(\frac{fmcap}{N_{ca}} \right)^{epcap} \quad N_{ca} \equiv \frac{k \nabla p}{\sigma_{wg}} \quad (3.1)$$

where σ_{wg} is water/gas interfacial tension and N_{ca} is capillary number. $fmcap$ represent the lowest reference capillary number for a given application. $epcap$ scales F_5 with changing pressure gradient and controls the non-Newtonian behavior in the low-quality regime. While equation (3.1) is an option for capturing shear dependent behavior in foams, we choose not to use it in this paper for two reasons: (1) it is most applicable in the low-quality foam regime while SAG injections operates mostly in the high-quality regime; (2) it is dependent dynamically on pressure gradient ∇P which is not utilized in FFT as the fractional-flow curves are calculated *a priori* and not dependent flow rate.

3.1.2. Radial Flow

In radial flow, however, shear rate is a function of radius (See section 2.5). Mobility must scale with position, and therefore, the fractional flow curve must change as well. Rossen et al. [13] propose an analytical closed-form solution for fractional-flow in the context of polymer injection where $f_w = f(S_w, x_D)$. The analytical solution, however, is limited to a non-Newtonian exponent of $n = 0.5$, and thus, is not universally applicable to our case.

In this paper, we take a more general approach by scaling $fmdry$ as a function of radius. The general form of a non-Newtonian model is a power-law fluid model in which viscosity depends on interstitial velocity, and through equation (2.22), inversely with radius

$$\mu = \mu^o \left(\frac{v}{v^o} \right)^{n-1} = \mu^o \left(\frac{r^o}{r} \right)^{n-1} \quad (3.2)$$

where μ^o is a reference viscosity at some reference velocity v^o . The parameter n is the fluid power-law exponent which controls rheology ($n < 1$ indicates a shear-thinning behavior, $n = 1$ indicates a Newtonian behavior, and $n > 0$ indicates a shear thickening behavior). As can be seen in equations (2.4-2.6), adjusting gas viscosity has the same effect on mobility ratio as the same adjustment to water relative permeability. Thusly,

$$\frac{\mu_g}{\mu_g^o} = \left(\frac{r^o}{r}\right)^{n-1} = \frac{k_{rw}}{k_{rw}^o} \quad (3.3)$$

Plugging in equation (2.7) and canceling terms yields

$$\left(\frac{r^o}{r}\right)^{n-1} = \frac{(S_w - S_{wr})^{nw}}{(S_w^o - S_{wr})^{nw}} \quad (3.4)$$

As previously mentioned, $fmdry$ is essentially the water saturation at which foam collapses. Substituting in $fmdry$ for S_w values in equation (3.4), taking the reference location to be the outer radius r_e , and rearranging leads to

$$fmdry(r) = S_{wr} + (fmdry_e - S_{wr}) \left(\frac{r}{r_e}\right)^{\frac{n-1}{n_w}} \quad (3.5)$$

where $fmdry_e$ is a reference $fmdry$ value at outer radius r_e .

3.2. Semi-Empirical Solution Method

With $fmdry$ a function of radius as in equation (3.5), the foam fractional-flow equation is now a function of radius as well. In the context of Buckley-Leverett analysis, this implies that characteristic lines in $x_D - t_D$ space curve as they move outward. In addition, the shock front velocity changes as the fractional-flow curve shifts as a function of position. In order to capture this change, we take a semi-analytical approach. The flow domain ($x_D \in [0, 1]$) is discretized into many layers, each of which are assigned an $fmdry$ value based on equation (3.5). For each layer, an individual fractional-flow curve is constructed with equation (2.34). Within each layer, standard Buckley-Leverett analysis as outlined in section 2.9.3 can be conducted. At the inlet, a number of characteristics are initialized with saturations ranging from S_{wr} to S_w^f . These characteristics locations in $x_D - t_D$ space are solved outward-in-space-forward-in-time by performing standard Buckley-Leverett analysis sequentially in each layer.

3.2.1. Space-Time Diagram Solution Algorithm

The general process for computing the $x_D - t_D$ diagram is as follows. Fractional flow curves are constructed for each layer. The shock saturation and fractional flow is calculated by solving for the point of tangency to the f_w curve for a line passing through point (1, 1). The root the function

$$f_w^f + \frac{df_w^f(S_w)}{dS_w}(1 - S_w) - 1 = 0 \quad (3.6)$$

is determined numerically using the `fzero` function in MATLAB, an iterative solver which uses a combination of bisection, secant, and inverse quadratic interpolation methods. This derivative of the fractional flow equation is calculated analytically as

$$\frac{df_w^f}{dS_w} = \frac{\lambda_{rg}^f(S_w)\lambda'_{rw}(S_w) - \lambda_{rw}(S_w)\lambda'_{rg}(S_w)}{(\lambda_{rw}(S_w) + \lambda_{rg}^f(S_w))^2} \quad (3.7)$$

The derivatives for gas and water relative mobilities with respect to water saturation are

$$\lambda'_{rw}(S_w) = \frac{n_w k_{rw}^o \left(\frac{S_w - S_{wr}}{1 - S_{wr} - S_{gr}}\right)^{(n_w - 1)}}{\mu_w (1 - S_{wr} - S_{gr})} \quad (3.8)$$

$$\lambda'_{rg}(S_w) = \frac{n_g k_{rg}^o \left(\frac{1 - S_w - S_{wr}}{1 - S_{wr} - S_{gr}}\right)^{(n_g - 1)}}{\mu_g (1 - S_{wr} - S_{gr})} \quad (3.9)$$

The derivative of the foam relative mobility is

$$\lambda_{rg}^f(S_w) = FM'(S_w)\lambda_{rg}(S_w) + FM(S_w)\lambda_{rg}'(S_w) \quad (3.10)$$

The derivative of the foam mobility reduction factor (FM) is

$$FM'(S_w) = -\frac{FM^2 \times fmmob \times epdry}{\pi(1 + epdry^2(S_w - fmdry)^2)} \quad (3.11)$$

A range of points on the fractional-flow curve between S_{wr} and S_w^{sf} are selected; these points initialize the characteristics that are tracked in the $x_D - t_D$ plane. For the first characteristic, the velocity (i.e., slope) at the characteristic water saturation is calculated with equation (3.7). The dimensionless time of the characteristic is then calculated at the edge of the first layer by rearranging equation (2.35) to solve for dimensionless time as a function of position. When this characteristic moves into the next layer with a shifted fractional-flow curve, f_w is the quantity that is conserved, not S_w . The point shifts to the right or left, keeping the same value of f_w but at a new water saturation. The velocity of this point is calculated once again, and the dimensionless time at the edge of the second layer is calculated. The characteristic continues to move from layer to layer, calculating the new t_D at the edge of each layer with

$$t_D|_c^l = \frac{\Delta x_D|_c^l}{f_w'(S_w|_c^l)} + t_D|_c^{l-1} \quad (3.12)$$

where subscript c denotes a given characteristic and superscript l denotes layer number. Once the characteristic reaches the edge of the domain ($x_D = 1$), the process repeats for the each characteristic until the $x_D - t_D$ diagram is complete. The same procedure is also conducted for the shock-front line.

Additional bookkeeping also needs to occur depending on whether a shear-thinning or shear-thickening case is occurring. In the shear-thinning case, characteristics curve upward (increasing velocity) and collide with the shock-front line which is curving downward (decreasing). If a characteristic collides with the shock-front in a given layer, the collision is noted and the characteristic does not propagate to the next layer. For the shear-thickening case, characteristics curve downward (decreasing velocity) while the shock-front curves upward (increasing velocity). Characteristics do not collide, but peel of the shock-front line moving outward in space. In this case, a new characteristic line is created and tracked in space-time starting at the (S_w^{sf}, f_w^{sf}) point in each layer.

3.2.2. Time Rediscritization

The solution process outlined above results in dimensionless times for each characteristic line at regularly spaced intervals in x_D (i.e. layer boundaries). In order to calculate dimensionless pressure drop as a function of time, however, the position of each characteristic with a given total relative mobility must be known at each point in time. To achieve this, the $x_D - t_D$ diagram is re-sampled at discrete points in dimensionless time. Since characteristics are lines within each layer (constant velocity), linear interpolation is used to calculate dimensionless position within layers. The position of the shock-front is also resampled as a function of time. After the dimensionless breakthrough time, a *pseudo-characteristic* point is calculated at the outlet ($x_D = 1$) at each t_D , and assigned a total relative mobility which is a linear interpolation between total relative mobilities of the characteristics between which the outlet point falls.

3.2.3. Dimensionless Pressure Calculation

The dimensionless position of each characteristic at each sampled dimensionless time is calculated using equation (2.35) as follows

$$r = \sqrt{x_D(r_e^2 - r_w^2) + r_w^2} \quad (3.13)$$

By using average mobilities between two consecutive characteristics at two consecutive radii, the pressure drop between each characteristic is estimated by

$$p^{i+1} - p^i = \frac{Q_t}{2\pi kh} \frac{1}{2} \left(\frac{1}{\lambda_{rt}^i} + \frac{1}{\lambda_{rt}^{i+1}} \right) \ln \left(\frac{r^{i+1}}{r^i} \right) \quad \text{for } i = 1 \dots M \quad (3.14)$$

where P^1 and r^1 are the pressure and radius at the wellbore, and P^M and r^M are the pressure and radius at the shock-front. The total pressure difference between the wellbore to the shock radii ($P_{r_w} - P_{r_{shock}}$) is calculated by the summation of all the *inter-characteristic* pressure increments. The numerical integration of equation (2.28) is therefore

$$\Delta P_f = P_{r_w} - P_{r_{shock}} = \frac{q_t}{2\pi h k} \int_{r_{shock}}^{r_w} \frac{1}{r \lambda_{rt}^f(S_w)} dr = \sum_{i=1}^M (P^{i+1} - P^i) \quad (3.15)$$

Ahead of the foam bank, the pressure drop is that caused by the water bank at initial conditions as in equation (2.24)

$$\Delta P_w = P_{r_{shock}} - P_{r_e} = \frac{Q_t}{2\pi h k \lambda_{rw}} \ln\left(\frac{r_e}{r_{shock}}\right) \quad (3.16)$$

The total pressure drop, therefore, is the sum of the foam bank and water bank pressure drops normalized to that of water injection as follows

$$P_D = \frac{\Delta P_f + \Delta P_w}{\frac{Q}{2\pi k h \lambda_{rw}} \ln\left(\frac{r_e}{r_w}\right)} \quad (3.17)$$

Equation (3.17) can be used to calculate the total dimensionless pressure drop as a function of dimensionless time.

4

Results

The results of the following scenarios are presented in this chapter.

1. Berea core with Newtonian foam behavior ($n=1$)
2. Berea core with shear-thickening foam behavior ($n=1.6$)
3. Berea core with shear-thinning foam behavior ($n=0.38$)

All cases were run with the Corey relative permeability parameters and foam parameters presented for the Berea core in Al Ayesh [2]. The power-law exponents for shear thickening and shear-thinning regimes were average values Berea core trials in the high-quality and low-quality regimes respectively [3]. Cases were run with 50 layers and 100 characteristic points initially below the shock spaced reverse logarithmically. Layer spacing was linear, and t_D timestep for time resampling was 0.01. Wellbore radius was 0.1m and outer radius was 100m.

4.1. Newtonian Case

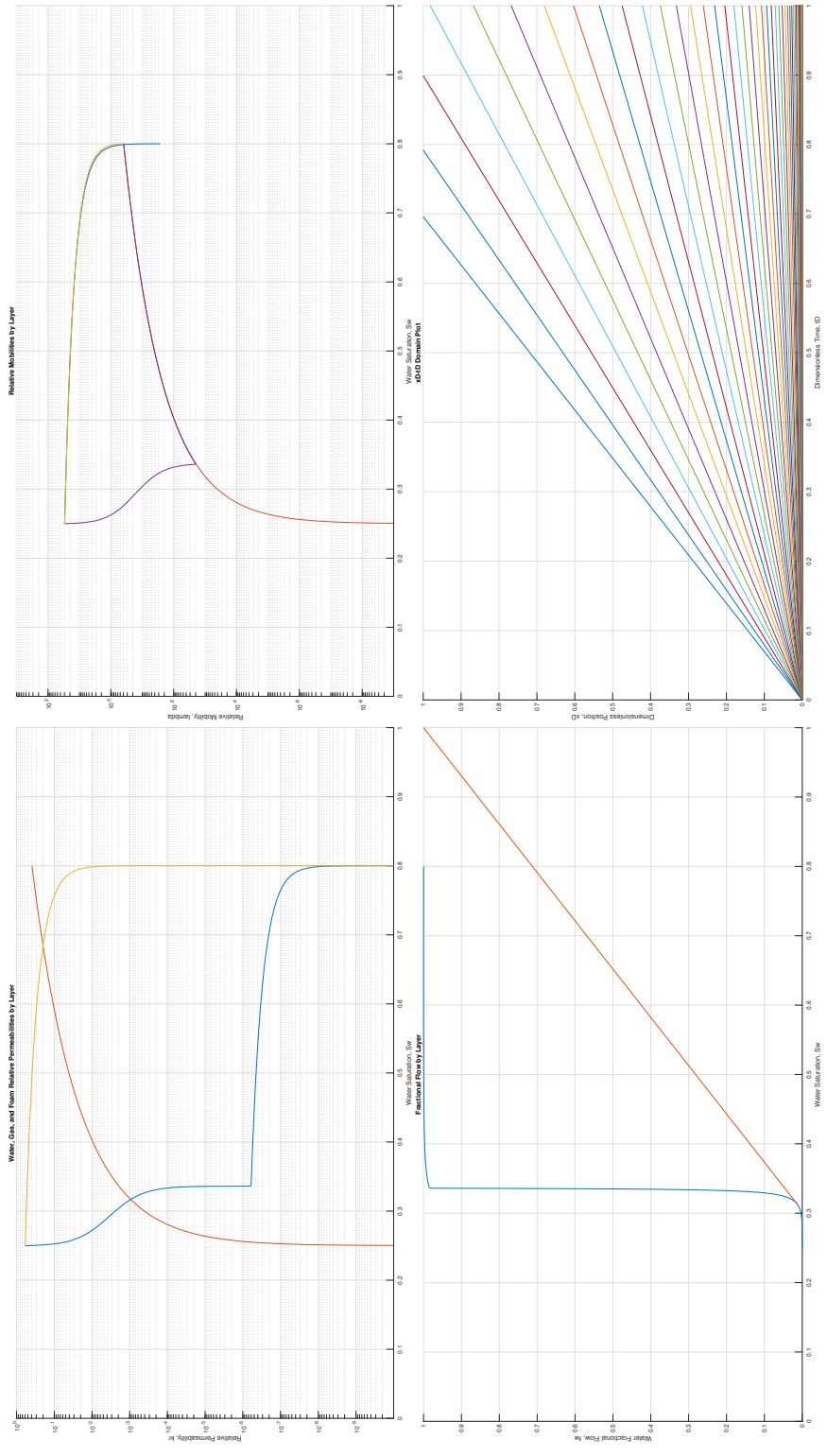


Figure 4.1: Buckley-Leverett Plots for Newtonian Berea

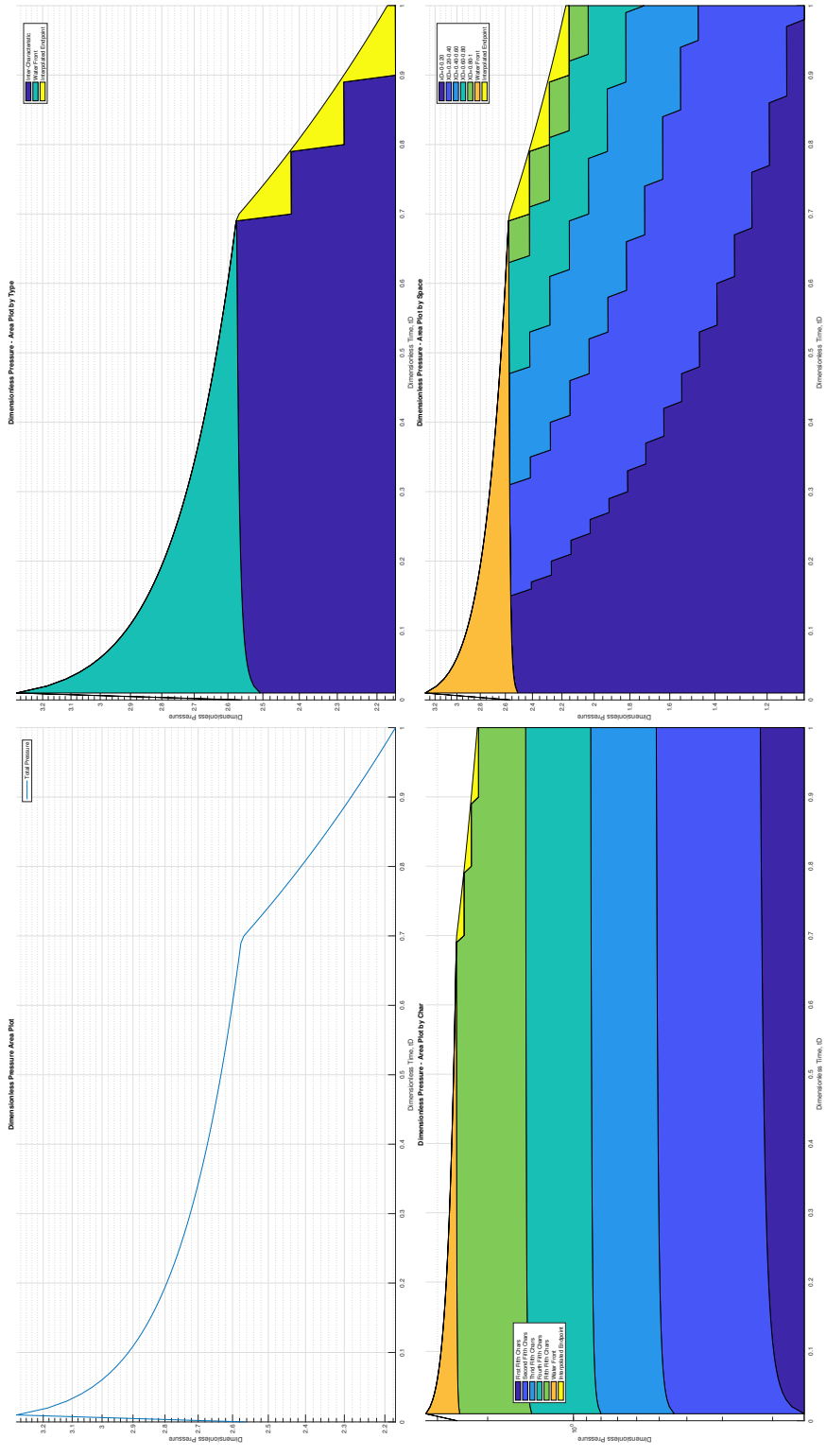


Figure 4.2: Dimensionless Pressure Plots for Newtonian Berea

4.2. Shear Thickening Case

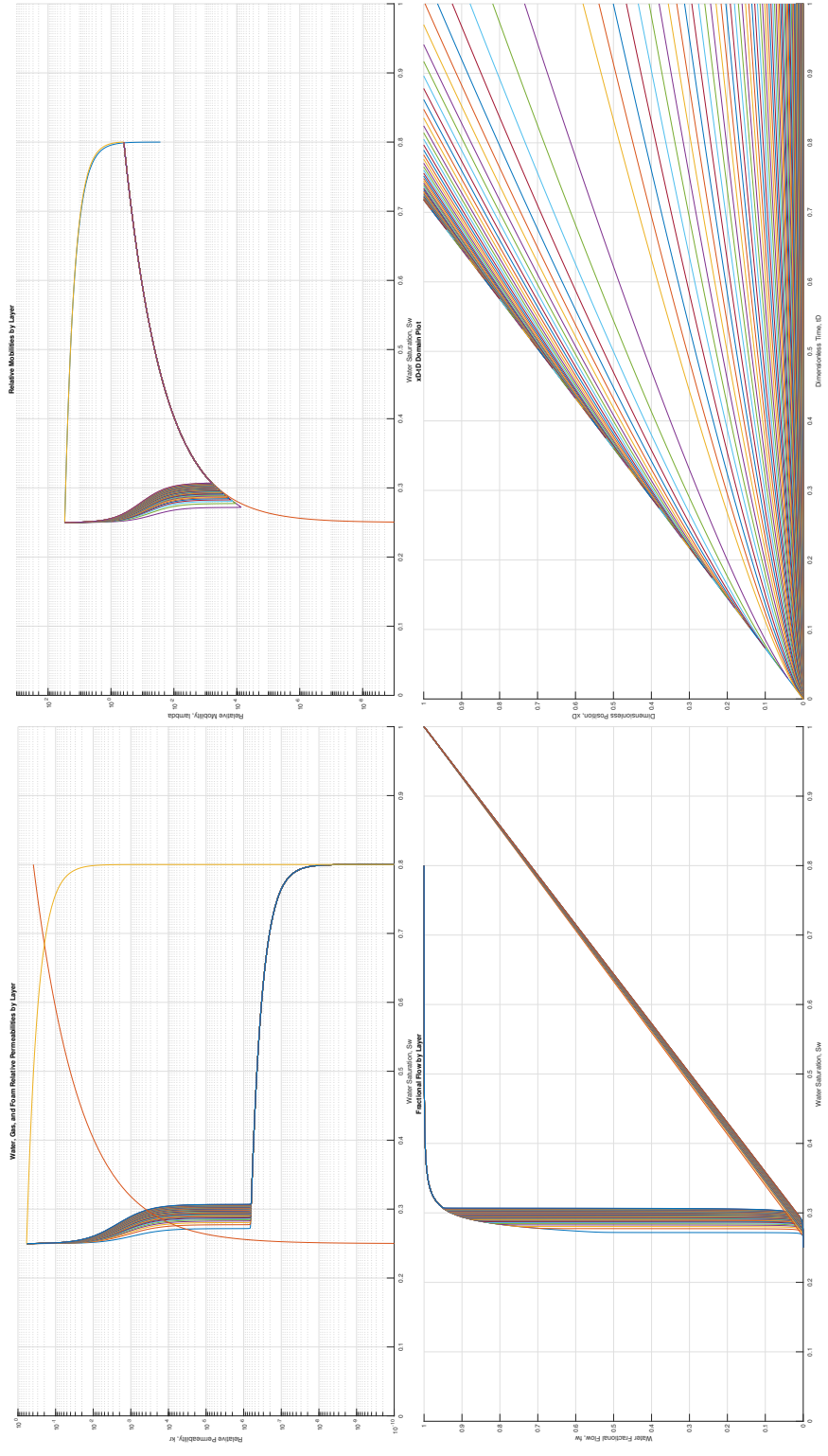


Figure 4.3: Buckley-Leverett Plots for Shear-Thickening Berea

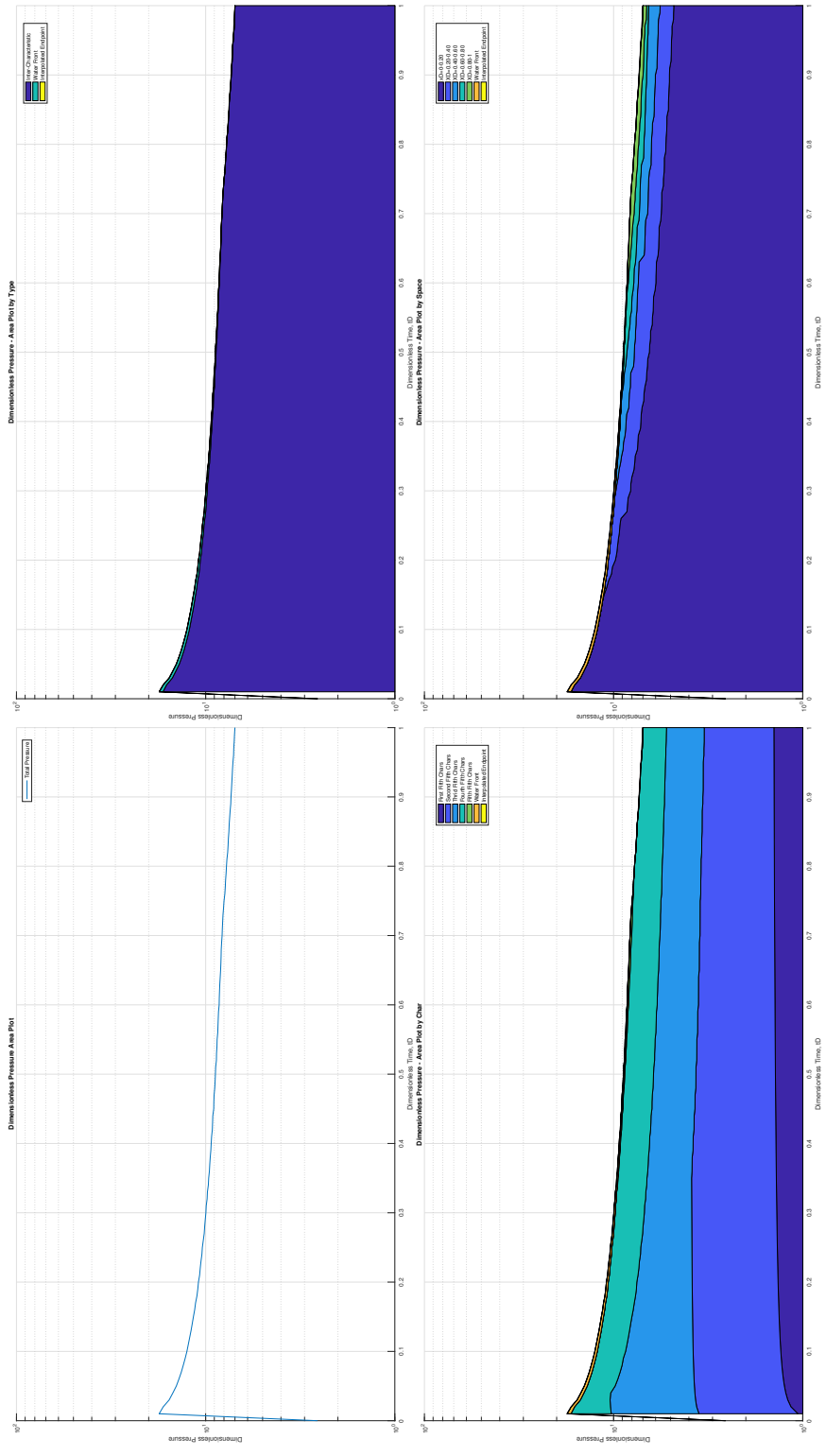


Figure 4.4: Dimensionless Pressure Plots for Shear-Thickening Berea

4.3. Shear Thinning Case

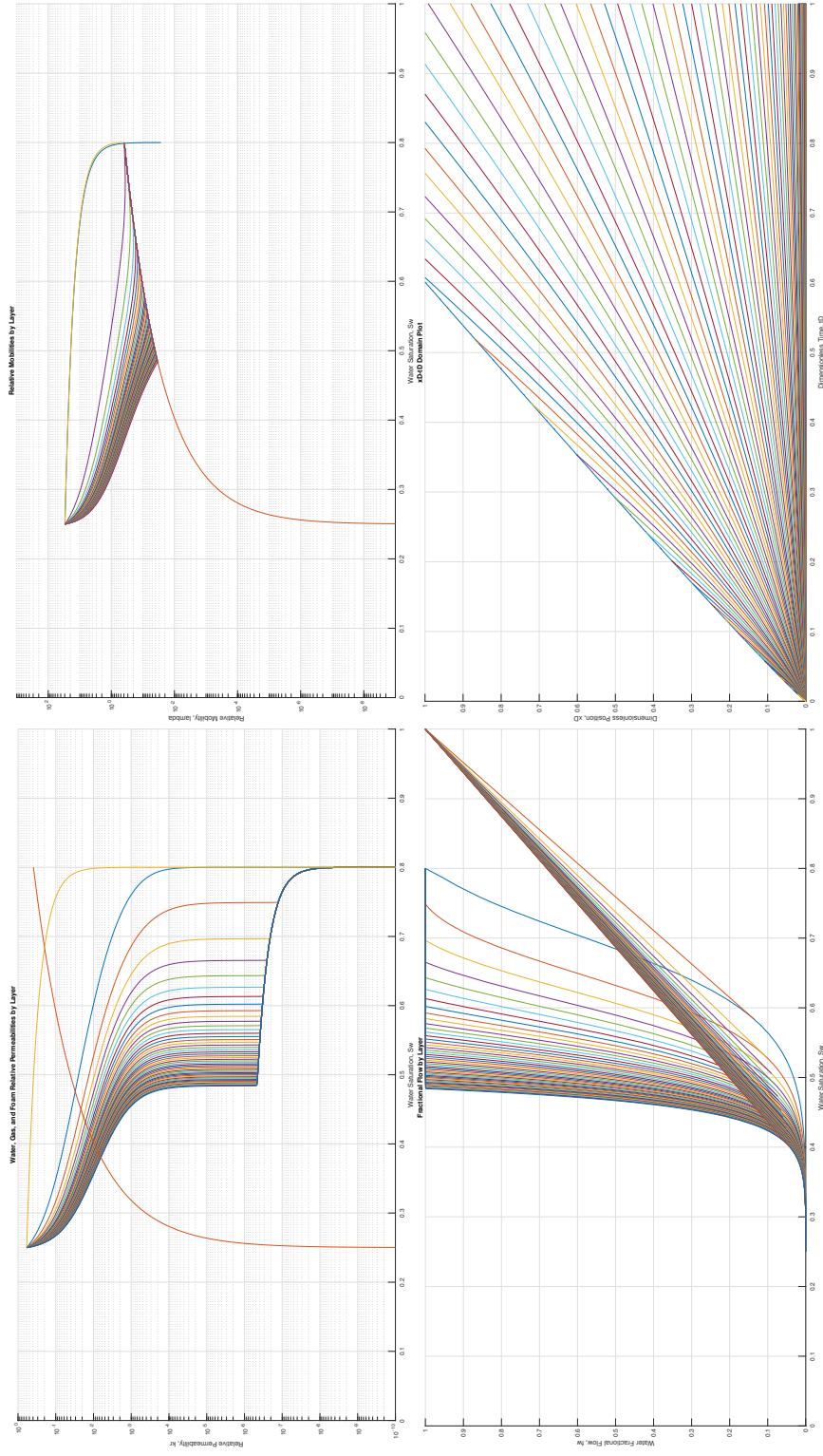


Figure 4.5: Buckley-Leverett Plots for Shear-Thinning Berea

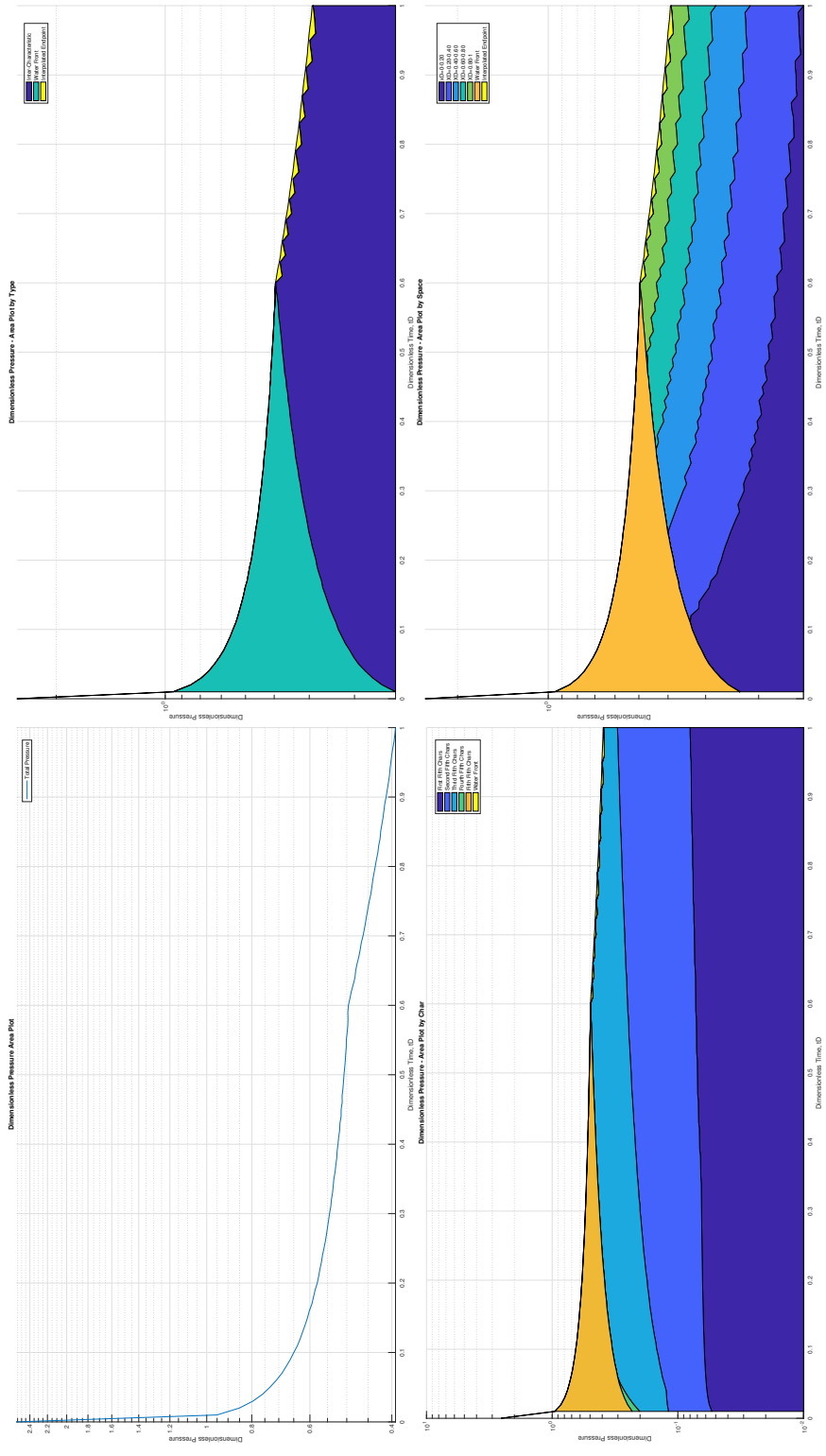


Figure 4.6: Dimensionless Pressure Plots for Shear-Thinning Berea

5

Discussion and Conclusions

The results presented above demonstrate that this semi-analytical Buckley-Leverett process can be used to capture the effects of non-Newtonian rheologies in SAG foam injection. In the Newtonian case, characteristics are straight as expected. It is also interesting to note that pressure drop across the foam front is relatively constant for the majority of injection until breakthrough, as was predicted by Boeije and Rossen [4]. P_D initially declines quickly, shallows out near breakthrough, but drops off after breakthrough. Dimensionless pressure in the shear-thickening case is an order of magnitude higher than the Newtonian case, such that the pressure drop almost negligible. The majority of pressure drop occurs in the first 20% of the flow domain, much more significantly than in the Newtonian case. The shear-thinning case shows improved injectivity an order of magnitude less than the shear-thickening case and even less than the Newtonian case. Pressure drop across the foam bank actually increases from the start of injection to breakthrough. This could be an important design consideration when dealing with shear-thinning foams. While injectivity on whole is much more favorable, the raise in pressure drop across the foam bank could require increased injection rates over time. Facilities would need to be designed to handle the increased capacity. Additionally, pressure drop is spread out across a much larger range of the reservoir, which could help with viscous instabilities within the foam-bank.

The non-Newtonian Buckley-Leverett process developed in this paper could be extended in further work in multiple ways. More tuning of the foam parameters should be done to obtain more scalable results to the field. The process could be combined with the work presented in Al Ayesh [2] to investigate how non-Newtonian rheologies influence diversion in a heterogeneous reservoir. The influence of the presence of oil could also be integrated into the model to help more realistically predict field performance.

Bibliography

- [1] Fundamentals of enhanced oil recovery. OCLC: ocn892537734.
- [2] A.H. Al Ayesh. Optimal SAG design in heterogeneous reservoirs. URL <http://repository.tudelft.nl/islandora/object/uuid:d2d395a1-3cb5-43e6-88bd-c2e7b0ce88af?collection=education>.
- [3] J.M. Alvarez, H.J. Rivas, and W.R. Rossen. Unified model for steady-state foam behavior at high and low foam qualities. 6(3):325–333. ISSN 1086-055X. doi: 10.2118/74141-PA. URL <http://www.onepetro.org/doi/10.2118/74141-PA>.
- [4] Christian S. Boeije and William Rossen. Gas-injection rate needed for SAG foam processes to overcome gravity override. 20(1):049–059. ISSN 1086-055X. doi: 10.2118/166244-PA. URL <http://www.onepetro.org/doi/10.2118/166244-PA>.
- [5] S.E. Buckley and M.C. Leverett. Mechanism of fluid displacement in sands. 146(1):107–116. ISSN 0081-1696. doi: 10.2118/942107-G. URL <http://www.onepetro.org/doi/10.2118/942107-G>.
- [6] L. Cheng, S.I. Kam, M. Delshad, and W.R. Rossen. Simulation of dynamic foam-acid diversion processes. Society of Petroleum Engineers. doi: 10.2118/68916-MS. URL <http://www.onepetro.org/doi/10.2118/68916-MS>.
- [7] Computer Modeling Group Ltd. *CMG-STARs User's Guide*.
- [8] Henry Darcy. *Les fontaines publiques de la ville de Dijon*.
- [9] Larry W. Lake. *Enhanced oil recovery*. Society of Petroleum Engineers. ISBN 978-1-55563-305-9. OCLC: 934758173.
- [10] Eduardo Jose Manrique, Charles Philip Thomas, Ravi Ravikiran, Mehdi Izadi Kamouei, Michael Lantz, Jorge Luis Romero, and Vladimir Alvarado. EOR: Current status and opportunities. Society of Petroleum Engineers. doi: 10.2118/130113-MS. URL <http://www.onepetro.org/doi/10.2118/130113-MS>.
- [11] Maryam Namdar Zanganeh. Simulation and optimization of foam EOR processes. OCLC: 840445422.
- [12] Gary A. Pope. The application of fractional flow theory to enhanced oil recovery. 20(3):191–205. ISSN 0197-7520. doi: 10.2118/7660-PA. URL <http://www.onepetro.org/doi/10.2118/7660-PA>.
- [13] W. R. Rossen, A. Venkatraman, R. T. Johns, K. R. Kibodeaux, H. Lai, and N. Moradi Tehrani. Fractional flow theory applicable to non-newtonian behavior in EOR processes. 89(2):213–236, . ISSN 0169-3913, 1573-1634. doi: 10.1007/s11242-011-9765-2. URL <http://link.springer.com/10.1007/s11242-011-9765-2>.
- [14] W.R. Rossen and M.W. Wang. Modeling foams for acid diversion. 4(2):92–100. ISSN 1086-055X. doi: 10.2118/56396-PA. URL <http://www.onepetro.org/doi/10.2118/56396-PA>.
- [15] W.R. Rossen, Z.H. Zhou, and C.K. Mamun. Modeling foam mobility in porous media. 3(1):146–153, . ISSN 1076-0148. doi: 10.2118/22627-PA. URL <http://www.onepetro.org/doi/10.2118/22627-PA>.
- [16] Zuhui Zhou and W.R. Rossen. Applying fractional-flow theory to foam processes at the "limiting capillary pressure". 3(1):154–162. ISSN 1076-0148. doi: 10.2118/24180-PA. URL <http://www.onepetro.org/doi/10.2118/24180-PA>.